Queensland University of Technology
Brisbane Australia

This may be the author's version of a work that was submitted/accepted for publication in the following source:

Wang, Xiaodong
(2021)
Simultaneous measurement of pole figure and residual stress for polycrystalline thin films - -' compensated GID in side-inclination mode.
Journal of Applied Crystallography, *54*(5), pp. 1424-1436.

This file was downloaded from: https://eprints.qut.edu.au/213719/

© Consult author(s) regarding copyright matters

This work is covered by copyright. Unless the document is being made available under a Creative Commons Licence, you must assume that re-use is limited to personal use and that permission from the copyright owner must be obtained for all other uses. If the document is available under a Creative Commons License (or other specified license) then refer to the Licence for details of permitted re-use. It is a condition of access that users recognise and abide by the legal requirements associated with these rights. If you believe that this work infringes copyright please provide details by email to qut.copyright@qut.edu.au

License: Creative Commons: Attribution-Noncommercial 4.0

Notice: *Please note that this document may not be the Version of Record (i.e. published version) of the work. Author manuscript versions (as Submitted for peer review or as Accepted for publication after peer review) can be identified by an absence of publisher branding and/or typeset appearance. If there is any doubt, please refer to the published source.*

https://doi.org/10.1107/S1600576721008335

Journal of Applied Crystallography research papers

Simultaneous measurement of pole figure and residual stress for polycrystalline thin films — *ω-φ'* compensated GID in side-inclination mode

Authors

Xiaodong Wang[ab]*

[a]Central Analytical Research Facility, Queensland University of Technology, Level 6, P Block, Gardens Point Campus, Brisbane, Queensland, 4001, Australia

[b]Centre for Materials Science, Queensland University of Technology, Level 6, P Block, Gardens Point Campus, Brisbane, Queensland, 4001, Australia

Correspondence email: tony.wang@qut.edu.au

REVIEW DOCUMENT

Synopsis A new GID geometry between in-plane and out-plane is proposed for simultaneous pole figure and residual stress measurement for polycrystalline thin films. Automatic data processing models are developed with refraction corrections implemented.

Abstract A new GID (Grazing Incident Diffraction) measurement geometry between in-plane and out-plane is proposed. It is improved from the previous *ω-φ* compensated GID in side-inclination mode for measurement of residual stress in polycrystalline thin films (Wang & van Riessen, 2018). Instead of keeping the constant azimuthal direction of the incident beam on thin film sample, the current proposed variation maintains a constant azimuthal direction of the scattering vector projection on the thin film sample. The variation is named as "*ω-φ′* compensated GID in side-inclination mode", which enables d-spacing measurements along the same azimuthal direction. An Excel spreadsheet is attached for readers to plan the measurement and to calculate the residual stress for the planned sample azimuthal direction. Anisotropic residual stresses of a polycrystalline NiFe thin film on Si *001* substrate are measured by combining this method with Phi rotations. Highly automatic data analyses templates are developed using DIFFRAC.TOPAS v7 launch mode to calculate residual stress for all planned azimuthal directions sequentially. A pole figure file in simple text format is also generated from the same dataset using DIFFRAC.TOPAS v7 launch mode, and can be directly imported into DIFFRAC.TEXTURE v4.1 for further texture analysis. Corrections for the incident beam refraction have been implemented in both data analyses models.

Keywords: polycrystalline thin film; residual stress; texture; TOPAS; GID

IMPORTANT: this document contains embedded data - to preserve data integrity, please ensure where possible that the IUCr Word tools (available from http://journals.iucr.org/services/docxtemplate/) are installed when editing this document.

Nomenclature of angles

Name	Symbol	Meaning
Theta	θ	Half of 2θ, which is the angle between the incident X-ray beam direction and the receiving X-ray beam direction of the detector;
Omega	ω	The angle between the incident X-ray beam and the alignment direction on the sample stage;
Bragg angle	θ_{hkl}	When $\omega = \theta_{hkl}$, a sample crystal plane of Miller index *hkl* diffracts X-ray to a direction forming $2\theta_{hkl}$ angle from the primary X-ray beam direction;
Detector	2θ-ω	The angle between the receiving X-ray beam direction of the detector and the alignment direction on the sample stage;
-	α	The actual incident angle between the primary X-ray beam and the thin-film surface;
Chi	χ	The Chi drive on a Eulerian cradle tilts the normal of sample surface out of the goniometer plane by an angle χ;
Phi	ϕ	The Phi drive on a Eulerian cradle rotates the sample around its surface normal;
	φ	The change of azimuthal direction of the primary X-ray beam after χ tilt;
-	φ'	The change of azimuthal direction of the scattering vector after χ tilt;
-	φ''	The change of azimuthal direction of the secondary X-ray beam after χ tilt;
-	β	The take-off angle of the secondary beam from the thin-film surface;
Psi	ψ	The angle between the scattering vector and the thin-film surface normal;
-	γ	The offset angle between the scattering vector and the sample stage normal when $\chi=0$, $\gamma=\theta_{hkl}-\omega$.

1. Introduction

In recent years, the addition of an “in-plane arm” or a “non-coplanar arm” to vertical goniometers has been adopted by diffractometer manufacturers (Inada, 2008; Product News, 2019). Measuring pole figure for bulk and thin film samples using the combined positioning of the in-plane arm and the detector arm has since been promoted, mainly due to the improved grain statistics by using the full line focus beam, without the need of an X-Y oscillator for point focus beam. However, the large beam footprint on the sample also enforces a restriction on the detection system: it requires an in-plane soller slit (in-plane Parallel Slit Analyzer) been placed in front of detector to resolve intensity along the in-plane $2\theta_{\chi}$ scanning direction. Phi scans at a fixed detector position limits this geometry to be a 0D texture measurement, the background level of which needs be measured separately. One issue of this geometry is its non-constant 2θ angular resolution, due to the orientation change of the in-plane soller slit with respect to the Debye cone (Fig. 1). This means the geometry is inefficient in recording 2θ peak profiles, especially at the low $2\theta_{\chi}$ angle regions (position 2 in Fig. 1(a)). It is quite often that textured samples are also under residual stress. If the 2θ angle is not optimised at each Phi position for these samples, 0D texture measurements may not be able to capture the maximum intensity of the hkl reflection, which compromises the accuracy of the measured pole figure (Fig. 1(b)). This limitation also prevents it to be applied for residual stress measurement, where accurate measurements of d-spacings are required.

REVIEW DOCUMENT

In Fig. 1 (a), the detector with in-plane soller has highest 2θ angular resolution at position 1, where the in-plane soller slit is parallel to the Debye arc, which is perpendicular to the in-plane $2\theta_\chi$ scan direction. However, at position 2, this detection system has lowest 2θ angular resolution, due to lack of an equatorial soller. If a “2-3 mm” receiving slit (Nagao & Kagam, 2011) or an equatorial soller (Benediktovitch *et al.*, 2014) was also used together with an in-plane soller, the diffraction signals from the large footprint on the sample will be largely excluded, which was meant to be the advantage of this geometry. Reduced intensity might be compensated by elongated measurement time. What could not be easily solved in this geometry is its incapability of perpendicularly scan across the Debye arc at general position 3. Either detector scan or $2\theta_\chi$ scan results a wide peak profile and the 2θ peak position optimised from these scans will obviously change the planned ψ angle. Perpendicularly scanning across the Debye arc really requires simultaneous movement of in-plane $2\theta_\chi$ drive and the detector drive at certain speed ratio (green arrow from the circle centre in Fig. 1(b)), which varies with the ψ angle along the Debye arc. To the author’s best knowledge, this combined scanning is not yet available on any commercial diffractometer with in-plane arm.

To solve this problem, it is indispensable to orient the normal of the Miller plane to be measured in a proper goniometer plane. The previously reported “ω-φ compensated GID in side-inclination mode” (Wang & van Riessen, 2018) is quite suitable for this purpose. In this geometry (Fig. 2), 1D texture measurement (peak profile over 2θ is recorded) is achieved by scanning a 0D detector with an equatorial soller (a.k.a. Parallel Slit Analyser, PSA) perpendicularly cross the Debye arc at any planned ψ tilt. Since the whole peak profile together with its background can be measured, this geometry is able to measure 2θ peak positions for residual stress analysis, and optimise 2θ peak intensities for pole figure measurement. Any diffractometer equipped with a Eulerian cradle, a point focus beam and an equatorial soller is able to perform such measurement.

Different to the method of scattering vector, around which the sample is rotated (Genzel, 1994), the “ω-φ compensated GID in side-inclination mode” was evolved from the original “GID in side-inclination method” (Ma *et al.*, 2002; Wang, Chuang*, et al.*, 2015; Wang, Huang*, et al.*, 2015), which combined the benefits of both GID method and side-inclination mode. GID (Grazing Incident Diffraction) shoots X-ray into a flat sample surface at a fixed shallow angle, and only scans detector to vary the 2θ angle. This geometry confines X-ray in thin film layers to maximise their interaction volume; the diffraction signals from substrates can then be supressed or avoided. Side-inclination, including Schultz (1949a, b) method using a divergent beam or χ mode (Section 3.1.2, Welzel *et al.*, 2005) using a parallel beam, employs an additional χ drive on a Eulerian cradle to freely select ψ angles. The ψ angle range in side-inclination mode is not restricted by the Bragg conditions in the equatorial plane as it is in the iso-inclination mode (a.k.a ω mode (Section 3.1.1, Welzel *et al.*, 2005)). The evolvement brought in by “ω-φ compensation” solved the issue of decreasing intensity by fixing the relative positions between the incident beam and the sample, through adjusting the ω and φ drives according to the χ tilts (Fig. 2). The equations describing these adjustments have been summarised previously (Wang & van Riessen, 2018).

REVIEW DOCUMENT

Although the "ω-φ compensation" geometry was initially improved from the *average* X-ray stress of polycrystalline thin films (a.k.a. AXS method, Wang, Chuang, *et al.*, 2015), it can be adapted to maintain a constant azimuthal direction of the scattering vector projection on the thin film plane, which extends its application to measure *anisotropic* surface residual stress of polycrystalline thin films. Since this measurement geometry is able to perpendicularly scan across any part of the Debye arc, accurate diffraction angles and intensities can be measured for crystal planes facing a range of ψ orientations on the upper hemisphere of the sample, which also allows deriving pole figure from the same dataset. This paper reports this adaption and its application on a polycrystalline NiFe layer on Si substrate.

2. Measurement Method

2.1. The original "ω-φ compensated GID in side-inclination mode" method

As pointed out in the previous report (Wang & van Riessen, 2018), the ω angle needs be increased to keep the actual incident angle α constant as χ tilts. The relationship among ω, φ, α and χ angles can be derived from the right angle tetrahedron EHIO in Fig. 3: The "ω-φ compensated GID in side-inclination mode" keeps the incident beam and the sample relatively stationary, through positioning the ω and ϕ drives according to equation (1) and (2). The X-ray always illuminates same sample volume regardless of χ tilts; the penetration depth of this geometry is not sensitive to χ tilts (See Section 2.4).

$$\omega = \arcsin\left(\frac{\sin\alpha}{\cos\chi}\right) \qquad 0 \le \chi \le 90° - \alpha, \alpha \le \omega \le 90° \tag{1}$$

$$\varphi = \arcsin(\tan\chi\tan\alpha) \quad 0 \le \chi \le 90° - \alpha, 0 \le \varphi \le 90° \tag{2}$$

For GID measurement, the actual incident angle α is usually small (normally lower than 3°, depends on thin film thickness). Fig. 4(a) and Fig. 4(b) plot the required adjustments of ω and φ according to the cradle χ tilt to maintain constant α angles. It is clear to see that these adjustments are minor until cradle χ tilts above 80°. Equation (1) and (2) show that ω and φ reach 90° when χ tilts to 90°-α. However, such high ω angle is only meaningful if a *hkl* reflection of $2\theta_{hkl} > 90°$ is measured, otherwise the diffracted beam will be below the sample surface hence not measurable (as Fig. 4(e) and equation (5) show below). In most case, pole figure measurement is for a reflection of low Miller index with $2\theta_{hkl} <$ 90°, therefore the maximum ω angle is limited to $2\theta_{hkl}$[1], which reversely restricts the maximum χ angle ($\chi_{\max} = \arccos(\sin\alpha/(\sin 2\theta_{hkl}))$) and the maximum achievable ψ angle ($\psi_{\max} = \arccos(\sin\alpha / (2\sin\theta_{hkl}))$) from equation (3) below).

As illustrated in the auxiliary right angle tetrahedron OABC in Fig. 3, the ψ angle monotonically increases with the cradle χ tilts:

$$\psi = \arccos(\cos\gamma\cos\chi) = \arccos(\cos(\theta_{hkl} - \omega)\cos\chi) \tag{3}$$

[1] Strictly speaking, finite detector sizes further limit the ω angle, as described in Appendix A.

REVIEW DOCUMENT

Considering $\alpha \leq \omega < 2\theta_{hkl}$, $\gamma = \theta_{hkl} - \omega$ is within the range of $(-\theta_{hkl}, \theta_{hkl} - \alpha]$, the ψ values calculated using equation (3) has a minimum value of $\theta_{hkl} - \alpha$. The ψ angle approaches the highest value of $\arccos(\sin\alpha/(2\sin\theta_{hkl}))$ as ω proceeds towards $2\theta_{hkl}$. As shown in Fig. 4(c), measuring peaks of lower Bragg angle θ_{hkl} can achieve a wider ψ coverage, which is preferred for residual stress measurement.

2.2. The "ω-φ' compensated GID in side-inclination mode" method

The original method described above measures diffraction signals from the same sample volume at different ψ angles (Fig. 2). The azimuthal direction of the scattering vector projection on the thin film plane change with χ tilts. As illustrated in the right angle tetrahedron AGFO in Fig. 3, $\overrightarrow{\mathrm{OG}}$ represents the projection of the scattering vector $\vec{q} = \overrightarrow{\mathrm{OA}}$ on the thin film plane. The relationship between the azimuthal direction of $\overrightarrow{\mathrm{OG}}$, $\angle\mathrm{GOF} = \varphi'$, and the ψ angle as well as the offset angle γ is:

$$\varphi' = \arccos(\sin(\theta_{hkl} - \omega)/\sin\psi) \tag{4}$$

Combining equation (3) and (4), the trend of φ' on χ tilts is shown in Fig. 4(d). Note equation (4) is considered to be superior than the previously reported tangent form of φ', as detailed in Appendix B.

If the cradle Phi drive is also rotated to follow this change of φ' angle ($\phi = \varphi'$), the projection of scattering vector on the thin film sample can be kept in the same azimuthal direction, which is required when measuring the lattice strain along certain sample direction. This method is proposed as "*ω*-*φ'* compensated GID in side-inclination mode" in this paper, which is illustrated in Fig. 5.

And by planning Phi rotation steps relative to the φ' angle calculated in equation (4) ($\phi = \varphi'$+360°/n), the d-spacings and intensities of the *hkl* reflection in all the azimuthal directions of the sample can be measured, which allow the derivation of both anisotropic surface residual stress and a pole figure. The planned pole figure orientations using the previous "*ω*-*φ* compensation" and the currently proposed "*ω*-*φ'* compensation" are compared in Fig. 6. Although both methods measure the same ψ coverage, it is clear to see the currently proposed "*ω*-*φ'* compensation" method (Fig. 6(b)) measures d_{hkl} along constant azimuthal directions of the sample, from which the residual stresses along these planned azimuthal directions can be derived, while the previous method (Fig. 6(a)) can only derive an average surface residual stress.

The take-off angle β of the diffracted beam with respect to the thin film surface and the azimuthal direction angle φ'' of the diffracted beam projected on the thin film surface can be linked to the cradle χ tilts from the right angle tetrahedron DOKL in Fig. 3, considering $\angle\mathrm{DOK} = 2\theta_{hkl} - \omega$:

$$\beta = \arcsin(\sin(2\theta_{hkl} - \omega)\cos\chi) \tag{5}$$

$$\varphi'' = \arctan(\tan(2\theta_{hkl} - \omega)\sin\chi) \tag{6}$$

As shown in Fig. 4(e), β decreases monotonically with the cradle χ tilt. As discussed in Appendix A, practically the minimum take-off angle β should allow the detector sensor to be fully above the thin film plane. The same restriction applies to the evolvement of φ'' angle, as shown in Fig. 4(f). The

REVIEW DOCUMENT

maximum ω_{max} and χ_{max} values calculated in the practical consideration in Appendix A guarantees φ'' angle is always positive.

2.3. Refraction correction for the incident beam

The refraction effect of the secondary beam can be omitted because the take-off angles (see β values calculated in the example of Table 1) are much larger than the critical angle α_c, which can either be calculated from the refraction index of the thin film material (Pavlinsky, 2007), or conveniently measured using X-ray Reflectometry (Appendix C). Refraction of the incident beam happens in the plane of △EOH in Fig. 3 when the incident angle α is close to the critical angle α_c. The refracted incident angle in the thin film layer would be $\alpha_r = \sqrt{\alpha^2 - \alpha_c^2}$, which is smaller than α. Since the planned incident angle α and critical angle α_c are both constant in this geometry, the refracted incident angle α_r is also a constant throughout the measurement. The actual scattering vector $\overrightarrow{q'}$ of the crystals is out of the goniometer plane and is closer to the thin film plane, as shown in Fig. 7.

Assuming all the wave vectors $\vec{k}$ have unity modulus, the vectors in Fig. 7 can be represented as:

$$-\overrightarrow{k_i} = [0, \cos\alpha, \sin\alpha];\ -\overrightarrow{k_i'} = [0, \cos\alpha_r, \sin\alpha_r];\ where\ \alpha_r = \sqrt{\alpha^2 - \alpha_c^2}$$

$$\overrightarrow{k_f} = [\cos\beta\sin(\varphi + \varphi''), -\cos\beta\cos(\varphi + \varphi''), \sin\beta];$$

$$\vec{q} = \overrightarrow{k_f} - \overrightarrow{k_i} = [\cos\beta\sin(\varphi + \varphi''), \cos\alpha - \cos\beta\cos(\varphi + \varphi''), \sin\alpha + \sin\beta];$$

$$\overrightarrow{q'} = \overrightarrow{k_f} - \overrightarrow{k_i'} = [\cos\beta\sin(\varphi + \varphi''), \cos\alpha_r - \cos\beta\cos(\varphi + \varphi''), \sin\alpha_r + \sin\beta]$$

Therefore the actual Psi angle between the measured crystal plane and the thin film surface plane is

$$\psi_{\text{act}} = \arccos\left(\frac{\overrightarrow{\text{OC}} \cdot \overrightarrow{q'}}{|\overrightarrow{\text{OC}}||\overrightarrow{q'}|}\right) = \arccos\left(\frac{\sin\alpha_r + \sin\beta}{\sqrt{2 + 2\sin\alpha_r\sin\beta - 2\cos\alpha_r\cos\beta\cos(\varphi + \varphi'')}}\right) \quad (7)$$

Equation (7) reduces to equation (3) when the refraction of the incident beam can be ignored (i.e. $\alpha_r = \alpha$).

The projection of $\overrightarrow{q'}$ on the thin film plane $\overrightarrow{\text{OG}'}$ and the vector $\overrightarrow{\text{OI}}$ in Fig. 3 can also be expressed as vectors in the sample coordinates XOY, to calculate φ'_{act}:

$$\overrightarrow{\text{OG}'} = [\cos\beta\sin(\varphi + \varphi''), \cos\alpha_r - \cos\beta\cos(\varphi + \varphi''), 0];$$

$$\overrightarrow{\text{OI}} = [-\cos\omega\sin\varphi, \cos\omega\cos\varphi, 0]$$

$$\varphi'_{\text{act}} = \arccos\left(\frac{\overrightarrow{\text{OG}'} \cdot \overrightarrow{\text{OI}}}{|\overrightarrow{\text{OG}'}||\overrightarrow{\text{OI}}|}\right) = \arccos\left(\frac{\cos\alpha_r\cos\varphi - \cos\beta\cos\varphi''}{\sqrt{\cos^2\alpha_r + \cos^2\beta - 2\cos\alpha_r\cos\beta\cos(\varphi + \varphi'')}}\right) \quad (8)$$

When the refraction can be ignored (i.e. $\alpha_r = \alpha$), equation (8) reduces to equation (4).

And the actual 2θ angle equals:

$$2\theta_{\text{act}} = \arccos\left(\frac{\overrightarrow{k_f} \cdot \overrightarrow{k_i'}}{|\overrightarrow{k_f}||\overrightarrow{k_i'}|}\right) = \arccos(\cos\alpha_r\cos\beta\cos(\varphi + \varphi'') - \sin\alpha_r\sin\beta) \quad (9)$$

It should be note that equation (9) derived here is considered to be the general form of refraction correction between in-plane GID and out-plane GID. In typical out-plane GID geometry, $\varphi = \varphi'' = 0$; equation (9) reduces to $2\theta_{\text{act}} = \alpha_r + \beta$; where the refraction effect has the largest impact to the 2θ

measurement. In typical in-plane GID geometry, $\alpha_r \approx \beta \approx 0°$, equation (9) reduces to $2\theta_{\text{act}} = \varphi + \varphi''$, where 2θ measurement is barely impacted by the refraction effect.

2.4. Penetration depth

Same as the previously reported *ω-φ* compensated GID in side-inclination mode (Wang & van Riessen, 2018), the currently proposed *ω-φ′* compensated GID in side-inclination mode is also a geometry between in-plane and out-plane. In most of the time, the diffraction plane (△DOE in Fig. 7) containing both primary and secondary beams is neither perpendicular nor parallel to the sample surface plane (△XOY in Fig. 7). However, the penetration depths of both geometries still follow the conventional penetration depth equation for GID method (Delhez *et al.*, 1987; Van Acker *et al.*, 1994; Welzel *et al.*, 2005; Birkholz *et al.*, 2006):

$$\tau_{63} = \frac{\sin\alpha \sin\beta}{\mu(\sin\alpha + \sin\beta)} \tag{10}$$

where μ represents the linear absorption coefficient of the thin film material under the radiation used. 63% of the diffracted intensity comes from top layer of depth τ_{63}. Combining equation (5) and equation (10), the penetration depths of the current proposed geometry can be plotted as Fig. 8 for different incident angles α. Compared with the penetration depth in the convictional side-inclination mode, the proposed geometry is able to probe surface sensitive information.

3. Experiment

3.1. Instrument Configuration

A Bruker D8 Advance diffractometer, equipped with a Cobalt X-ray twist tube oriented in point focus direction and operated in 35kV 40mA, was used to collect data of the proposed *ω-φ′* compensated GID in side inclination mode, as described in Section 2. A Φ0.5 mm micro-slit pinhole was plugged in the primary slit module, followed by a Φ0.5 mm collimator, to define the cross-section diameter of the incident point focus beam. The distance of these two pinholes is 115 mm, which gives the beam divergence around 8.7 mrad. A ~650 nm thick NiFe f.c.c. (face centre cubic) thin-film grown on a Si *001* substrate (thickness measured using AFM is provided in Appendix D) was mounted on a Compact Cradle Plus stage of D8 Advance. Other than a thin film height alignment, the thin film surface normal was also aligned in the Phi axis of this cradle (Appendix E), to maintain the GID incident angle after ϕ rotation. A 0.3° equatorial soller (PSA) of 20 mm opening was used to select parallelly diffracted X-rays to reach a LynxEye XE-T energy-dispersive detector, which is working at a narrow energy window to remove any non-diffraction photons. The detector was operated in zero-dimensional (0D) mode, with all the channels opened. The parallel beam on the receiving side can accommodate the height variations of the diffracting crystals in the thin film at high χ tilts.

REVIEW DOCUMENT

3.2. Implementation of the measurement method

The equations (1-9) are used in Table 1 to plan the measurement of the *111* reflection of NiFe thin film in different directions using the proposed geometry. An Omega-Phi^Prime.xlsx file available in the Supporting Information has equations (1-9) implemented to facilitate readers planning ω and φ' angles according to a desired actual incident angle α and a series of cradle tilt χ angles. The NiFe *111* reflection was measured using 2θ scan from 49 to 55°2θ at a step size of 0.05°2θ, which recorded more than 16 data points above FWHM of the *111* reflection profile. The dwell time was 3 seconds per step; each profile was measured in 360 seconds. In total 324 profiles (2θ measurements looped on 36 ϕ orientations, then looped on 9 χ tilts, as shown in Fig. 6(b)) were executed.

It can be seen from Table 1 that the differences between ψ' and the refraction corrected ψ'_{act} values increases up to around 0.1° with χ tilts, while the refraction correction on φ' angles are quite minor. The last column of Table 1 verifies the analysis of equation (9) in Section 2.3 that the refraction induced 2θ shift are more obvious at low χ tilts, and can be up to 0.1°, which is basically the value of α - α_r.

The ω, χ, φ' values calculated in Table 1 can be manually typed in measurement software like DIFFRAC.WIZARD as multiple methods in a single .bsml experiment file for the machine to execute. A more elegant way to achieve an auto-calculation of these driver positions is to implement the equation (1), (3) and (4) into a measurement script using DIFFRAC.COMMANDER -> Script Designer. The equation part of the implemented script is shown in Fig. 9, where the two layers of loops are defined. The full script is also available in the Supporting Information for Bruker diffractometer users. The script was then loaded in START JOBS to execute this measurement batch, together with a basic High Resolution XRD .bsml method, in which the hardware settings, the sample Z height and the 2θ scanning range were defined. The X-ray tube shutter was not closed between each scan, to minimise any unnecessary wearing of the shutter mechanism.

4. Results and Analyses

4.1. Pole Figure generation

The 324 measured *111* reflection profiles of the NiFe (f.c.c.) thin film in all orientations (9 χ tilts * 36 ϕ directions, available in the Supporting Information) were simultaneously fitted in DIFFRAC.TOPAS v7 software, using an INP file with equations (1-8) implemented (provided in Appendix F) to output a 3 column (chi, phi, intensity) pole figure file in .txt format, within 10 seconds on a computer with an Intel i7-3770 CPU. The exported pole figure file can be directly imported in DIFFRAC.TEXTURE V4.1 (Fig. 10(a)), which allows further texture analysis using either component modelling or spherical harmonics modelling. An example of component modelling is shown in Fig. 10(b), with the difference plot shown in Fig. 10(c). The high intensities of *111* reflection in pole figure form two circles at different ψ angles, indicating a weak texture of this NiFe thin film. It needs be noted that at least 3 *hkl* pole figures should be measured to define the Orientation Distribution Function (ODF) for a cubic phase.

REVIEW DOCUMENT

The pole figure simulation for NiFe *111* pole figure shown in Fig. 10(b) only serves as an example of further pole figure analysis.

As described in equation (3), ψ has a minimum value of $\theta_{hkl} - \alpha$, which means the centre low ψ region of pole figure cannot be measured, in return for the grazing incident geometry. The explicit .txt format can also be loaded in many other texture analysis software, after simple format conversions. Note that most of the texture software define the "RD" direction as 0° of the azimuthal direction, and the positive Phi direction as counter-clockwise direction. The INP file in Appendix F has devised a conversion from the Phi values defined in equation (8) to the Phi axis defined in texture software, so that the generated pole figure reflects the same sample mounting orientation as shown in Fig. 6(b).

4.2. Residual Stress analysis

The DIFFRAC.TOPAS INP file shown in Appendix G use recursive macros to selectively load and fit the NiFe *111* peak positions measured along same azimuthal direction (radially aligned directions highlighted in orange in Fig. 6(b) as well as their opposite directions). The d-spacings along φ and φ+180° directions are treated as the positive and negative sides of the same azimuthal direction. Refraction corrected $2\theta_{\text{act}}$ values are calculated using the equations (1-9) implemented in this INP file. Equation (11) shows the linear relationship between strain ε and $\sin^2\psi$ along one azimuthal direction, from the slope of which the residual stress σ can be derived:

$$\frac{\lambda/2/\sin 2\theta_{\text{act}} - d_0}{d_0} = \varepsilon = \frac{1+\upsilon}{E}\sigma \sin^2\psi - \frac{2\upsilon}{E}\sigma \quad (11)$$

where λ stands for the radiation wavelength, d_0 the unstrained interplanar distance of the same reflection, ε the d-spacing strain, υ the known Poisson ratio and E the known Young's modulus of the phase, σ the residual stress value in question. The slope equation of linear regression is used to calculate the normal residual stress value and its refinement error for the azimuthal direction, according to equations (12):

$$\frac{1+\upsilon}{E}\sigma = \frac{\sum_{i=1}^{n} \varepsilon_i \sin^2\psi_i - n\bar{\varepsilon}\,\overline{\sin^2\psi}}{\sum_{i=1}^{n}(\sin^2\psi_i)^2 - n\left(\overline{\sin^2\psi}\right)^2} \quad (12)$$

where $\bar{\varepsilon}$ and $\overline{\sin^2\psi}$ stands for the mean values of strains ε_i and the mean values of $\sin^2\psi_i$.

The INP file shown in Appendix G also automatically apply above operations for all the 18 azimuthal directions sequentially, using the multiple execution feature of DIFFRAC.TOPAS provide by the "*num_runs*" and "*Run_Number*" keywords.

The calculated tensile stress values for different azimuthal directions of the NiFe thin film sample are plotted in Fig. 11. It can be seen that these residual stress values are relatively uniform in the range between 460 MPa to 620 MPa, with errors around ±50 MPa, and their mean value around 530 MPa. The penetration depth τ_{63} of the measured tensile stress above can be read out from Fig. 8. Considering $\alpha_r = 0.8925°$, $\mu_{\text{NiFe}} = 595.6$ cm^{-1}, τ_{63} is calculated to be 255 nm.

An Omega-Phi^Prime.xlsx file is available in the Supporting Information. It also has the equations (1-14) implemented for readers who do not have access to TOPAS software to plan the measurement and

REVIEW DOCUMENT

calculate the residual stress, though the calculation only processes measured d-spacings for one azimuthal direction.

5. Discussion

5.1. Basic and recommended instrument configurations

In fact, the proposed ω-φ' compensated GID in side-inclination mode can be performed on any X-ray diffractometer, including systems with a horizontal goniometer, as far as a point focus beam, a Eulerian cradle and a secondary equatorial soller (PSA) can be mounted. The cross-section of the point focus beam needs be in round shape, therefore taking a small part of the reflected beam from a Göbel mirror is not suitable for this measurement. A primary poly-capillary module is recommended as it can converge more photons in point focus beam of lower beam divergence. A dedicated micro-focus source or an Excillum® MetalJet could largely improve the flux density of the point focus beam, which can shorten the measurement time. Although only χ and ϕ drives on the cradle stage are looped in this measurement, a motorised Z drive could largely facilitate the height alignment of thin film surface. The manual tilt alignment described in Appendix E is restricted to thin film samples of high reflectivity for visible laser. Any motorised double tilt attachment (e.g. Zeta-Xi or RxRy) on Eulerian cradle are recommended to automatically perform the tilt alignment for thin film on wedged substrates. It should be note that the positive direction of ϕ drive on the cradle is defined as clockwise (Fig. 3). A negative mark should be added to the calculated φ positions if this method is implemented on diffractometers with anti-clockwise Phi drive. There is little requirement on the X-ray detector; any 0D detector or detector that has 0D function can record the diffracted intensities behind an equatorial soller. Nevertheless, any means of secondary monochromation suitable for parallel X-ray beam is recommended to remove non-diffraction photons.

5.2. Advantages of the proposed geometry

Other than the benefits (e.g. able to perpendicularly scan across Debye arc) mentioned in Section 1 over the use of an "in-plane arm" or a "non-coplanar arm", the ω-φ' compensated GID is also superior than the conventional $\theta/2\theta$ measurement in side-inclination mode for polycrystalline thin films. Using a fixed incident angle of point focus beam relative to the thin film surface guarantees a fixed sample illumination length and volume as well as a fixed penetration depth. This makes the defocusing correction and the absorption correction, commonly required in the conventional side-inclination thin film texture measurement (Schulz, 1949b, a; Section 3.1.2, Welzel *et al.*, 2005; Section 3.2.1.4, Suwas, 2014), unnecessary in the proposed method. The long sample illumination length (28.6 mm = 0.5mm/sin1°) surveys larger number of crystals on the surface hence provides better crystal statistics, comparing to a symmetric $\theta/2\theta$ scan using point focus beam of same size. Since the constant penetration depth can be planned using equation (10) before the experiment, stress depth profiling for thin films or

bulk samples is also possible using different actual incident angle α in this geometry, although a dedicated micro-focus source mentioned above with narrower beam divergence might be required for better control of the incident angle.

In conventional out-plane GID, a secondary equatorial soller of small opening could crop intensity especially when scanned to close to 90 °2θ, as it may not be able to fully receive all the diffraction beam from the illuminated sample, which is usually long in GID. However, this limitation does not affect the proposed geometry, because the same 2θ angle was measured at different χ tilts. Beam cropping by the secondary equatorial soller, if there is any, should be constant therefore not cause intensity difference over different χ tilts.

In the conventional $\theta/2\theta$ measurement in side-inclination mode using point focus beam, the maximum ψ (=χ) tilt is barely beyond 75° due to gradually severe beam defocusing (Section 3.2.1.4, Suwas, 2014). The ω-φ' compensated GID method in side-inclination mode can easily reach ψ as high as 85° for pole figure measurement (as the lowest detector position calculated in Appendix A) without any intensity correction, because the same actual incident angle α is used throughout the measurement.

5.3. Limitations of the proposed geometry

Due to the use of point focus beam and 0D detection of wide parallel reflections, relative low diffraction intensities need be measured step by step. This makes the data collection in the proposed geometry slower than other 1D/2D texture or residual stress measurement methods, which are mainly suitable for bulk samples. Although completely automatic, the 324 profiles collected in this example took nearly 33 hours. Using a dedicated micro-focus source of higher flux density can reduce the data collection time.

GID based method intrinsically cannot measure the low ψ region in a pole figure (Van Acker *et al.*, 1994), due to the coupling between ψ and the incident angle α: $\psi_{min} = \theta_{hkl} - \alpha$. Applying this method for multiple *hkl* reflections could allow the ODF of the phase been refined, which in term allows the pole figure near the Normal Direction (ND) be calculated.

The impact of the incident beam refraction on d-spacing measurement in this geometry is not uniform from low χ to high χ tilt. As demonstrated in this example, a low incident angle 1° was used, which is close to the critical angle (0.451°, Appendix C) of the NiFe thin film under CoKα radiation. Therefore, refraction correction cannot be ignored in the residual stress measurement using the proposed geometry. The general form of refraction correction between in-plane GID and out-plane GID is developed as the equation (9). According to its analysis in section 2.3, the refraction effect of incident beam pushes the measured 2θ to higher angles. This 2θ shift is more obvious at low ψ angles than at high ψ angles, hence, overestimates tensile stress or underestimates compressive stress, if the impact from incident beam refraction was not corrected. The INP file in Appendix E has equation (9) implemented to solve this issue.

6. Conclusion

REVIEW DOCUMENT

A new GID geometry between in-plane and out-plane is developed and implemented to simultaneously measure the pole figure and residual stress of an NiFe thin film on Si substrate. Highly automatic data analyses and report models were also developed in DIFFRAC.TOPAS software, using its pre-processing feature and recursive macros. The ω-φ' compensation GID geometry is expanded from previous ω-φ compensation GID which only measures average residual stress for polycrystalline thin films. Corrections for incident beam refraction were also implemented in above analyses models. This geometry and its data analyses models can easily be applied on other polycrystalline thin films.

Figure 1 (a) Combined positioning of the in-plane arm and the detector arm for pole figure measurement. Blue circle – the goniometer plane; Thin black circle – the in-plane scanning plane; Orange dash circle – Debye cone. (b) Actual Debye cone of stressed material (orange belt) and the planned unoptimized detector positions (along the blue circle). Black arrows: in-plane $2\theta_\chi$ drive; Blue arrows: Detector drive. Position 1: detector drive at 0°; Position 2: in-plane drive at 0°; Position 3: general detector position.

Figure 2 ω-φ compensated GID in side-inclination mode: from (a) to (c), ω and φ angles keeps increasing with χ tilts to maintain relatively stationary between the incident beam and the thin film sample. The footprint direction of incident X-ray on the sample is highlighted as black lines.

Figure 3 The geometric relationships among the angles defined in the “Nomenclature of angles”. Note: $\gamma = \theta_{hkl} - \omega$.

Figure 4 (a-b) The trend of $\omega(\chi)$ and $\varphi(\chi)$ in equations (1) and (2) for different α angles; (c-f) The trends of $\psi(\chi)$, $\varphi'(\chi)$, $\beta(\chi)$, $\varphi''(\chi)$ in equations (3-6) respectively for different θ_{hkl} angles, at $\alpha = 1°$.

Figure 5 ω-φ' compensated GID in side-inclination mode: from (a) to (c), ω and φ' angles keeps increasing according to the χ tilts to keep the projection of scattering vector on the thin film sample in the same azimuthal direction, which is highlighted as an orange line on the sample.

Figure 6 Planned orientations in pole figure (stereographic projection) for a reflection at $\theta_{hkl} = 26°$, $\alpha = 1°$, $\chi = 0°, 10°, ..., 80°$ using (a) ω-φ compensated GID in side-inclination mode, with the azimuthal directions of scattering vector in Fig. 2 highlighted in orange, and (b) ω-φ' compensated GID in side-inclination mode, with the azimuthal directions of scattering vector in Fig. 5 highlighted in orange. (RD: Rolling Direction, TD: Transverse Direction).

Figure 7 Drawing of the primary beam $\overrightarrow{k_i} = \overline{EO}$ and secondary beam $\overrightarrow{k_f} = \overline{OD}$ as well as the scattering vector $\vec{q} = \overline{OA}$ in sample coordinates (Thin film plane XOY, with $\overline{OH}$ defined as Y axis, $\overline{OC} = [0,0,1]$ is the thin film normal). The refracted incident beam $\overrightarrow{k_i'}$ and the actual scattering vector $\overrightarrow{q'}$ are shown in orange.

REVIEW DOCUMENT

Figure 8 The changes of the normalised penetration depth $\mu\tau_{63}$ on cradle χ tilts using the proposed geometry, for different actual incident angle α. The $\mu\tau_{63}$ in the conventional side-inclination mode is shown as the uppermost blue curve for comparison, $\theta_{hkl} = 26°$.

Figure 9 Implementation of equations (1, 3, 4) in the measurement script.

Figure 10 Pole figure visualisation and fitting in DIFFRAC.TEXTURE (TD: Transverse Direction; RD: Rolling Direction): (a) Imported pole figure generated by DIFFRAC.TOPAS; (b) Simulated pole figure; (c) Difference between (a) and (b).

Figure 11 Normal residual stress values for all azimuthal directions of the NiFe thin film sample. The refinement errors are shown as error bars.

Figure 12 Lowest detector position (smallest $2\theta_{hkl}$-ω_{max} angle) when (a) the corner "N" of a rectangular detector sensor, or (b) the edge of a round detector sensor, touches the tilted thin film plane.

Figure 13 Function $\varphi'(\chi)$ using (a) Welzel's formation (2005) and using (b) the piecewise formation above, at different θ_{hkl} values.

Figure 14 Fitting to the X-ray reflectometry curve of the NiFe thin film under CoKα radiation in Rigaku® GlobalFit v2.1.1. Intensity is shown in logarithmic scale.

Figure 15 Thin film thickness measurement using Bruker NanoScope Analysis v2.0. Left side: bare substrate; Right side: with thin film on.

Figure 16 (a) Thin film sample mounted on the MiSUMi® double tilt attachment GFWG30-30 on the D8 Compact Cradle Plus, (b) Double alignment lasers (green and red) from the D8 goniometer helps to align the thin film normal to the cradle Phi axis.

REVIEW DOCUMENT

Table 1 The ω, φ, φ', ψ, β, φ'' angles from equations (1-6) maintaining a constant incident angle α = 1° for 9 cradle χ tilts at 10° step and the φ'_{act}, ψ_{act}, $2\theta_{\mathrm{act}}$ angles from refraction corrections from equations (7-9). The planned $2\theta_{111}$ of the f.c.c. NiFe thin film is at 52°.

χ(°)	ω(°)	φ(°)	ψ(°)	φ'(°)	β(°)	φ''(°)	φ'_{act}(°)	ψ_{act}(°)	$2\theta_{\mathrm{act}}$(°)
0	1.0000	0.0000	25.0000	0.0000	51.0000	0.0000	0.0000	25.0537	51.8925
10	1.0154	0.1763	26.7917	20.4380	49.9223	12.0966	20.4364	26.8488	51.8942
20	1.0642	0.3640	31.5597	36.3388	46.8542	22.8502	36.3365	31.6254	51.8990
30	1.1547	0.5774	38.1987	47.1988	42.1871	31.5520	47.1964	38.2757	51.9069
40	1.3055	0.8392	45.8940	54.4211	36.3524	38.1383	54.4188	45.9830	51.9177
50	1.5558	1.1920	54.1849	59.3163	29.7088	42.8442	59.3141	54.2850	51.9310

60	2.0003	1.7325	62.8209	62.7924	22.5209	45.9044	62.7904	62.9305	51.9463
70	2.9249	2.7488	71.6600	65.6122	14.9763	47.3044	65.6103	71.7767	51.9634
80	5.7682	5.6812	80.6227	69.4819	7.2038	45.7935	69.4801	80.7439	51.9815

Acknowledgements The author would like to thank Dr. Yanan Xu in Central Analytical Research Facility (CARF), QUT to perform the AFM measurement. Dr. Stefan Jakobs in Bruker AXS is appreciated to provide a framework of the measurement script (.cs file).

REVIEW DOCUMENT

References

Benediktovitch, A., Ulyanenkova, T. & Ulyanenkov, A. (2014). *J. Appl. Crystallogr.* **47**, 1298–1303.

Birkholz, M., Fewster, P. F. & Genzel, C. H. (2006). *Thin Film Analysis by X-Ray Scattering*, Germany: Wiley-VCH.

Delhez, R., de Keijser, T. H. & Mittemeijer, E. J. (1987). *Surf. Eng.* **3**, 331–342.

Genzel, C. (1994). *physica status solidi (a)* **146**, 629-637.

Inada, K. (2008). *Rigaku Journal* **24**, 10–15.

Ma, C.-H., Huang, J.-H. & Chen, H. (2002). *Thin Solid Films* **418**, 73–78.

Nagao, K. & Kagam, E. (2011). *Rigaku Journal* **27**, 6–11.

Pavlinsky, G. V. (2007). *Fundamentals of X-Ray Physics*, pp. 124–157. Cambridge, United Kingdom: Cambridge International Science Publishing.

Product News (2019). *Journal of Failure Analysis and Prevention* **19**, 1583–1585.

Schulz, L. G. (1949a). *J. Appl. Phys.* **20**, 1030–1033.

Schulz, L. G. (1949b). *J. Appl. Phys.* **20**, 1033–1036.

Suwas, S. (2014). *Crystallographic Texture of Materials*, 1st ed. 2014. ed. London: Springer London.

Van Acker, K., De Buyser, L., Celis, J. P. & Van Houtte, P. (1994). *J. Appl. Crystallogr.* **27**, 56–66.

Wang, A.-N., Chuang, C.-P., Yu, G.-P. & Huang, J.-H. (2015). *Surf. Coat. Technol.* **262**, 40–47.

Wang, A.-N., Huang, J.-H., Hsiao, H.-W., Yu, G.-P. & Chen, H. (2015). *Surf. Coat. Technol.* **280**, 43–49.

Wang, X. & van Riessen, A. (2018). *Powder Diffr.* **32**, S9–S15.

Welzel, U., Ligot, J., Lamparter, P., Vermeulen, A. C. & Mittemeijer, E. J. (2005). *J. Appl. Crystallogr.* **38**, 1–29.

Appendix A.

Strictly, the maximum ω angle ω_{max} should be smaller than $2\theta_{hkl}$. This is because a 0D detector needs be fully opened in this geometry to maximise the measured intensity. In order to allow the whole sensor to be above the tilted thin film surface, the maximum ω angle is further limited according to the lowest detector position, which is reached when the corner of the detector sensor touches the tilted thin film plane, as shown in Fig. 12, depends on the sensor shapes.

Let $\delta = 2\theta_{hkl} - \omega_{max}$, in the triangle MNK′ of Fig. 12(a):

$$\angle \mathrm{MNK}' = \arctan\left(\frac{MK'}{MN}\right) = \arctan\left(\frac{R\sin\delta - (L/2)\cos\delta}{W/2}\right) = \chi_{max} \quad (13)$$

and in the triangle MNK′ of Fig. 12(b):

$$\angle \mathrm{MNK}' = \arctan\left(\frac{MK'}{MN}\right) = \arctan\left(\frac{R^2\sin\delta - r^2\cos\delta\cot\delta}{\sqrt{R^2r^2 - r^4\cot^2\delta}}\right) = \chi_{max} \quad (14)$$

where, R is the goniometer radius, W is the width of a rectangular sensor in goniometer axial direction, L is the length of the rectangular sensor in equatorial direction, r is the radius of a round sensor. Plugging equation (1) $\chi_{max} = \arccos\left(\frac{\sin\alpha}{\sin\omega_{max}}\right)$ into above equations, the value of ω_{max} can be derived for each scenario, which is much smaller than $2\theta_{hkl}$. In the f.c.c. NiFe example in this paper, R = 280 mm, L = 14.4 mm, W = 16 mm, $2\theta_{Fe111}$ = 52°, α = 1°, ω_{max} is solved to be 18.78° and χ_{max} = 86.89°, ψ_{max} = 86.91°, δ_{min} = 33.22°, β_{min} = 1.7°, φ'' reduced to 33.20°. The experiment planed in Table 1 is well within this limit. The Omega-Phi^Prime.xlsx file available in the Supporting Information also has equations (13-14) implemented to calculate the lowest detector position.

Combining equation (13) or (14) with equation (1) can also facilitate users to plan the maximum χ tilt for an In-plane GID experiment before the corner of detector sensor travels below the thin film plane at the staring angle $2\theta_{start}$. Particularly, plugging $\delta = 2\theta_{start} - \arcsin\left(\frac{\sin\alpha}{\cos\chi_{max}}\right)$ in equation (13) or (14) allows the solving of χ_{max}.

Appendix B.

The tangent form of φ' has been reported as equation (22) in section 3.1.3 "Combined ω/χ mode" in a previous review paper (Welzel *et al.*, 2005). The tangent formation in that paper leads to a non-continuous function at the point $\omega = \theta_{hkl}$ (Fig. 13(a)). This is because ω can be larger than θ_{hkl} at high χ tilt, which makes the φ' angle calculated using the arctan function negative, therefore an additional π rad needs be added on to make φ' a continuous function with the scenario of $\theta_{hkl} > \omega$:

$$\varphi' = \begin{cases} \arctan\dfrac{\sin\chi}{\tan(\theta_{hkl}-\omega)} & \theta_{hkl} > \omega \\ \pi/2 & \theta_{hkl} = \omega, \\ \arctan\dfrac{\sin\chi}{\tan(\theta_{hkl}-\omega)} + 90° & \theta_{hkl} < \omega \end{cases} \tag{15}$$

The piecewise form of above equation is the correct continuous function (Fig. 13(b)). However, the arccos form in the equation (4) derived in this paper is an even more concise continuous form of φ', because arccos function is able to return obtuse φ' angles (>90°), therefore is considered to be superior.

Appendix C.

The X-ray Reflectivity (XRR) curve of the NiFe thin film on silicon substrate used in this paper was collected using the same diffractometer described in Section 3.1. A parallel Göbel mirror converged divergent X-ray from the Cobalt Twist X-ray tube in line focus direction into a parallel beam before a 0.1 mm exit slit controlling the incident beam width. Two 0.1 mm slits were used in the secondary side to define the receiving beam direction. The LynxEye XE-T detector working in 0D mode was mounted on 90° position, in order to open all the channels to receiving X-ray reflections. This maximises the detector dynamic range, hence no filter or absorber was needed for the X-ray Reflectivity measurement. The NiFe thin film sample was aligned according to its specular reflection.
As no monochromator was used in this measurement, the XRR setup could not resolve oscillations from such thick thin film (See Appendix D). However, the critical angle of the NiFe thin film on silicon substrate under CoKα radiation can be seen from the "knee" of the curve, where X-ray starts to penetrate the surface layer. As shown in Fig. 14, the critical angle α_c is measured to be 0.902°/2 = 0.451°.

Appendix D.

Fig. 15 shows the thickness of the NiFe thin film, the step of which has been measured using Bruker® Dimension Icon PT AFM in PeakForce Tapping mode. The average film thickness was measured to be 648 nm.

Appendix E.

REVIEW DOCUMENT

An additional tilt correction is required to align the surface normal of any thin film on wedged substrate in the Phi axis direction of the D8 Compact Cradle Plus. A MiSUMi® double tilt attachment GFWG30-30 (inset of Fig. 16(a)) is found to have a suitable height and suitable screw size and pitch to be mounted on the Compact Cradle Plus of D8 Advance, as shown in Fig. 16(a). The double tilt attachment was adjusted so that the reflections of the double alignment lasers (green and red) on the goniometer to the roof corners of D8 Advance enclosure are stationary, while the thin film sample is spinning along the Cradle Phi drive (Fig. 16(b)).

Aligning the thin film surface normal in the phi axis direction also enables phi spinning to average any in-plane texture for conventional out-plane (coplanar) GID measurement.

Appendix F.

DIFFRAC.TOPAS features a pre-processing step for INP files before kernel treatment, which allows recursive macros in below INP file to simultaneously load and refine hundreds of 1D data as well as analyse and report their refinable parameters. Below INP file can be executed in either DIFFRAC.TOPAS v6 or v7 to generate a 3 column (Chi, Phi, Intensity) pole figure file (.txt format) which can be directly imported in DIFFRAC.TEXTURE v4.1 for further texture analysis.

```
'This INP file performs simultaneous fittings for 1D peak profiles (.xy) of same hkl looped on Phi
then looped on Chi. The data files need be named as “c_n”, in which “c” refers to any filename and ‘n’
refers to a continuous running number e.g. from 1 to Chi_Num*Phi_Num. Cf: X.Wang(2021) J.Appl.Cryst.

'macro Numeric(n) {#prm a = n; #out a} 'v7 TOPAS.inc already included this macro; uncomment this line
when running this INP in v6.

'Total 324 measured peaks (of 9 Chi tilts * 36 Phi directions)
#prm Chi_Num 9 ' please provide the number of Chi tilts
#prm Phi_Num 36 ' please provide the number of Phi directions
#prm Total_Num =Chi_Num*Phi_Num;

macro load_sequential_data(c,n,n2) '(c=any_filename, n=start_number, n2=finish_number)
{#m_if n>n2; #m_else
xdd c##_##n##.xy local Chi = 10 Round((n-(#out Phi_Num +1)/2)/#out Phi_Num); local Rotation = Mod((n-
1),#out Phi_Num)*10; Peak(n) 'The steps of both Chi tilts & Phi rotations are 10 deg
load_sequential_data(c,Numeric(n+1),n2)
#m_endif
}

macro Sum_up(c, n) {#m_if n<1; 0 #m_else c##_##n + Sum_up(c, Numeric(n-1)) #m_endif}
macro List_of(c, n) {#m_if n==1; c##_##1 #m_else c##_##n, List_of(c, Numeric(n-1)) #m_endif}
prm Average_Peak_Position = (Sum_up(peak_position, #out Total_Num) )/#out Total_Num;:1
prm Average_Peak_Intensity = (Sum_up(peak_intensity, #out Total_Num) )/#out Total_Num;:1
prm Min_Intensity =Min(List_of(peak_intensity,#out Total_Num));:1
prm Max_Intensity =Max(List_of(peak_intensity,#out Total_Num));:1
prm !alpha 1 'Please update the actual incident angle
prm !alpha_c 0.451 'Please update the critical angle for thinfilm (0 to neglect refraction correction)
prm !alpha_r = Sqrt(alpha^2 - alpha_c^2);:0.8925

out "pole_figure.txt" append
Out_String("TEXTURE      4.1\n")
Out_String("FILETYPE     POLEFIGURE\n")
Out_String("VERSION      1\n")
Out_String("TIMESTAMP    2021-04-18T14:36:41.0162969+10:00\n") 'Please update date and time
Out_String("#1   Experimental     ")
out_record out_fmt "%4.1f\t" out_eqn = Average_Peak_Position;
out_record out_fmt "%4.1f" out_eqn = Average_Peak_Position;
```

PREVIEW DOCUMENT

```
out_record out_fmt " °\t"
out_record out_fmt "%4.0f\t" out_eqn = #out Total_Num;
out_record out_fmt "%10.14f\t" out_eqn = Min_Intensity/Average_Peak_Intensity;
out_record out_fmt "%10.14f\t" out_eqn = Max_Intensity/Average_Peak_Intensity;
out_record out_fmt "%10.14f\t" out_eqn = Average_Peak_Intensity;
out_record out_fmt "%7.5f\n" out_eqn = 1.78898; 'Please provide radiation wavelength

'Load 324 peaks using the recursive macro
load_sequential_data(NiFe_Omega_Phi_Prime,1,#out Total_Num)

for xdds {
x_calculation_step 0.1
bkg @ 283.112828 9.446721166
LP_Factor( 0)
Radius(280)
CoKa7_Holzer(0.0001)  }

macro Peak(n) {
   xo_Is
   xo peak_position##_##n 51.82 'Please provide the initial 2Theta angle
      peak_type spv
         spv_h1 @ 0.4075754746
         spv_h2 @ 0.3601611893
         spv_l1 @ 0.6252098289
         spv_l2 @ 0.6942399704
   I peak_intensity##_##n 128
local Omega = ArcSin(Sin(alpha Deg)/Cos(Chi Deg)) Rad;:1 'Equation(1)
local Phi = ArcSin(Tan(Chi Deg) Tan(alpha Deg) ) Rad;:1 'Equation(2)
local Psi = ArcCos(Cos((peak_position##_##n /2 - Omega) Deg) Cos(Chi Deg)) Rad;:1 'Equation(3)
local Phi1 = ArcCos(Max(-1,Min(1,Sin((peak_position##_##n /2 - Omega)Deg)/Sin(Psi Deg)))) Rad;:1
'Equation(4)
local beta = ArcSin(Sin((peak_position##_##n - Omega) Deg) Cos(Chi Deg)) Rad;:1 'Equation(5)
local Phi2 = ArcTan(Tan((peak_position##_##n - Omega) Deg) Sin(Chi Deg)) Rad;:1 'Equation(6)
local Psi_act = ArcCos((Sin(alpha_r Deg)+Sin(beta Deg))/Sqrt(2 + 2 Sin(alpha_r Deg) Sin(beta Deg) - 2
Cos(alpha_r Deg) Cos(beta Deg) Cos((Phi + Phi2) Deg))) Rad;:1  'Equation(7)
local Phi1_act = ArcCos(Max(-1,Min(1,(Cos(alpha_r Deg)Cos(Phi Deg)-Cos(beta Deg) Cos(Phi2
Deg))/Sqrt((Cos(alpha_r Deg))^2+(Cos(beta Deg))^2-2 Cos(alpha_r Deg) Cos(beta Deg) Cos((Phi + Phi2)
Deg))))) Rad;:1 'Equation(8)
out_record out_fmt "%6.3f\t" out_eqn = Psi_act;
out_record out_fmt "%4.3f\t" out_eqn = 180 - Rotation + Phi1_act - Phi1; '180-Rotation+Equation(8)-
Equation(4)
out_record out_fmt "%10.15f\n" out_eqn =peak_intensity##_##n /Average_Peak_Intensity;}
```

Appendix G.

Since version 6, DIFFRAC.TOPAS includes "*num_runs*" and "*Run_Number*" keywords allowing an INP file to be executed multiple times. Combining this function with recursive macros defined in below INP file, the measured d-spacing values in same azimuthal direction are selected and simultaneously fitted, from which a residual stress value together with its refinement error are calculated and reported. The "*Run_Number*" value loops from 0 to "*num_runs*-1", which effectively processes all the azimuthal directions sequentially.

```
'This INP file performs simultaneous refinement sequentially. Residual stress values are refined from
Chi_Num*2 1D peak profiles (.xy) of same hkl for Phi_Num/2 azimuthal directions. D-spacings of Phi and
Phi+180deg are refined together as the - and + sides of same direction. The data files need be named
as "c_n", in which "c" refers to any filename and 'n' refers to a continuous running number. Cf:
X.Wang(2021)J.Appl.Cryst.
num_runs 18
do_errors
'macro Numeric(n) {#prm a = n; #out a} 'v7 TOPAS.inc already included this macro; uncomment this line
when running this INP in v6.

'Load 324 measured peaks (of 9 Chi tilts * 36 Phi directions)
#prm Chi_Num 9 'please provide the number of Chi tilts
```


REVIEW DOCUMENT

```
#prm Phi_Num 36 'please provide the number of Phi directions
#prm Total_Num =Chi_Num*Phi_Num;

macro load_spaced_data(c,n,n2,sp) '(c=any_filename, n=start_number, n2=finish_number, sp=load data
every sp step)
{#m_if n>n2; #m_else
xdd c##_##n##.xy local Chi = 10 Round((n-(#out Phi_Num +1)/2)/#out Phi_Num); local Rotation = Mod((n-
1),#out Phi_Num)*10; Peak(n) 'The steps of both Chi tilts & Phi rotations are 10 deg
load_spaced_data(c,Numeric(n+sp),n2,sp)
#m_endif
}

macro Sum_up(c, n) {#m_if n<1; 0  #m_else c##_##n + Sum_up(c, Numeric(n-#out Phi_Num/2)) #m_endif}
macro Sum_xy_up(c1,c2,n) {#m_if n<1; 0 #m_else c1##_##n c2##_##n + Sum_xy_up(c1,c2, Numeric(n-#out
Phi_Num/2)) #m_endif}
prm Average_SINPSI2 = (Sum_up(SINPSI2, Numeric(Run_Number+1+#out Phi_Num/2*(#out Chi_Num*2-1))
))/(#out Chi_Num*2);:1
prm Average_Strain_act = (Sum_up(Strain_act, Numeric(Run_Number+1+#out Phi_Num/2*(#out Chi_Num*2-1))
))/(#out Chi_Num*2);:1
prm Sum_xiyi = Sum_xy_up(Strain_act, SINPSI2, Numeric(Run_Number+1+#out Phi_Num/2*(#out Chi_Num*2-1))
);:1
prm Sum_xixi = Sum_xy_up(SINPSI2, SINPSI2, Numeric(Run_Number+1+#out Phi_Num/2*(#out Chi_Num*2-1))
);:1
prm Slope = (Sum_xiyi - Numeric(#out Chi_Num)*2 * Average_SINPSI2 * Average_Strain_act)/(Sum_xixi -
Numeric(#out Chi_Num)*2 * Average_SINPSI2 * Average_SINPSI2);:1 'Equation(12)
prm !nu 0.32 'Possion ratio
prm !YM 202429 'Young's modulus Unit: MPa
prm rs = Slope / (1+nu) * YM ; :700 'Residual Stress Unit: MPa
prm !alpha 1 'Please update the actual incident angle
prm !alpha_c 0.451 'Please update the critical angle for thinfilm (0 to neglect refraction correction)
prm !alpha_r = Sqrt(alpha^2 - alpha_c^2);:0.8925
prm !d0 2.04613

out "residual_stresses.txt" append
out_record out_fmt "%4.0f\t" out_eqn = 180-Mod(Run_Number,#out Phi_Num)*10;
out_record out_fmt "%10.5f\t" out_fmt_err "%10.5f\n" out_eqn = rs;

'Load 18 peaks along same azimuthal direction using the recursive macro
load_spaced_data(NiFe_Omega_Phi_Prime,Numeric(Run_Number+1),#out Total_Num,Numeric(#out Phi_Num/2))

for xdds {
x_calculation_step 0.05
'exclude 52.9 53.6
bkg @ 283.112828 9.446721166
LP_Factor( 0)
Radius(280)
CoKa7_Holzer(0.0001)  }

macro Peak(n) {
   xo_Is
   xo peak_position##_##n 51.71 'Please provide the initial 2Theta angle
      peak_type spv
         spv_h1 @ 0.4075754746
         spv_h2 @ 0.3601611893
         spv_l1 @ 0.6252098289
         spv_l2 @ 0.6942399704
      I peak_intensity##_##n 128
local Omega = ArcSin(Sin(alpha Deg)/Cos(Chi Deg)) Rad;:1 'Equation(1)
local Phi = ArcSin(Tan(Chi Deg) Tan(alpha Deg) ) Rad;:1 'Equation(2)
local Psi = ArcCos(Cos((peak_position##_##n /2 - Omega) Deg) Cos(Chi Deg)) Rad;:1 'Equation(3)
local Phi1 = ArcCos(Max(-1,Min(1,Sin((peak_position##_##n /2 - Omega)Deg)/Sin(Psi Deg)))) Rad;:1
'Equation (4)
local beta = ArcSin(Sin((peak_position##_##n - Omega) Deg) Cos(Chi Deg)) Rad;:1 'Equation(5)
local Phi2 = ArcTan(Tan((peak_position##_##n - Omega) Deg) Sin(Chi Deg) ) Rad;:1 'Equation(6)
local Psi_act = ArcCos((Sin(alpha_r Deg)+Sin(beta Deg))/Sqrt(2 + 2 Sin(alpha_r Deg) Sin(beta Deg) - 2
Cos(alpha_r Deg) Cos(beta Deg) Cos((Phi + Phi2) Deg))) Rad;:1  'Equation(7)
local Phi1_act = ArcCos(Max(-1,Min(1,(Cos(alpha_r Deg)Cos(Phi Deg)-Cos(beta Deg) Cos(Phi2
Deg))/Sqrt((Cos(alpha_r Deg))^2+(Cos(beta Deg))^2-2 Cos(alpha_r Deg) Cos(beta Deg) Cos((Phi + Phi2)
Deg))))) Rad;:1 'Equation(8)
local Theta2_act = ArcCos(Cos(alpha_r Deg) Cos(beta Deg) Cos((Phi + Phi2) Deg) - Sin(alpha_r Deg)
Sin(beta Deg)) Rad;:1 'Equation(9)
prm SINPSI2##_##n = (Sin(Psi_act Deg))^2;
prm Strain_act##_##n = (Lam/2/Sin(Theta2_act/2 Deg)-d0)/d0;
'Uncomment below lines to export detailed epsilon-SinPsi2 list
```

PREVIEW DOCUMENT

```
'out_record out_fmt "%10.15f\t" out_eqn = (Sin(Psi_act Deg))^2; 'Sin^2Psi
'out_record out_fmt "%10.15f\n" out_eqn = (Lam/2/Sin(Theta2_act/2 Deg)-d0)/d0; 'Actual d-spacing after
refraction correction
}
```

REVIEW DOCUMENT

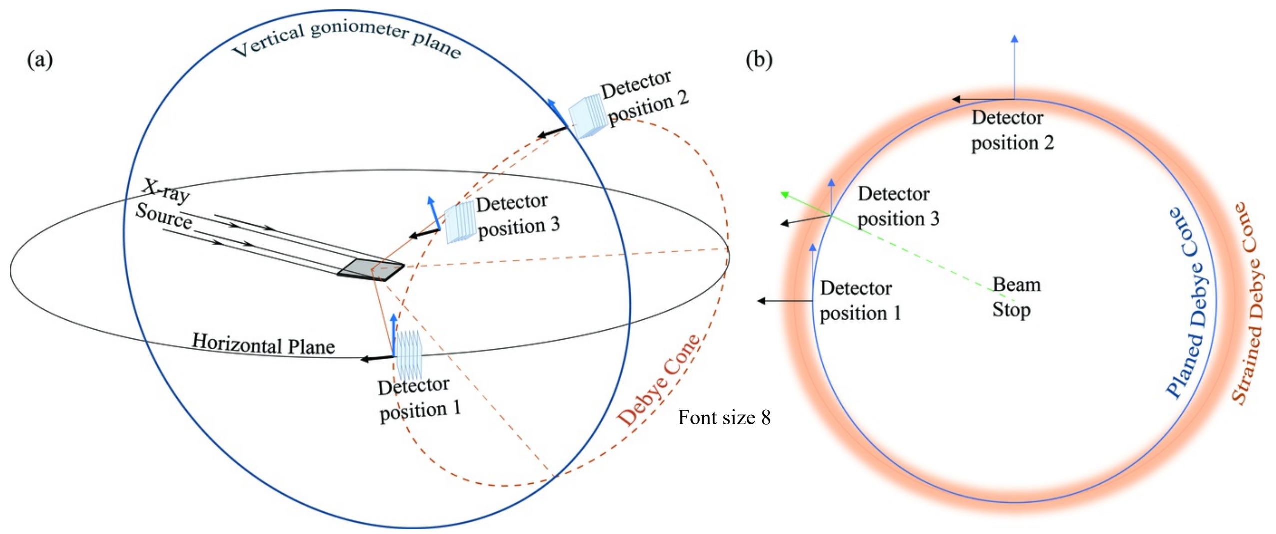

Figure 1

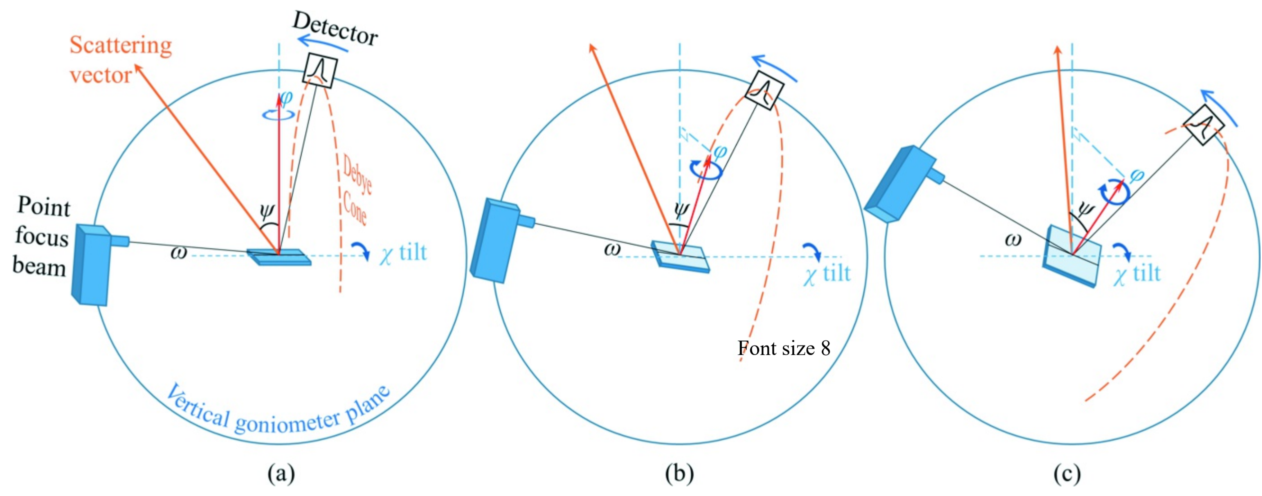

Figure 2

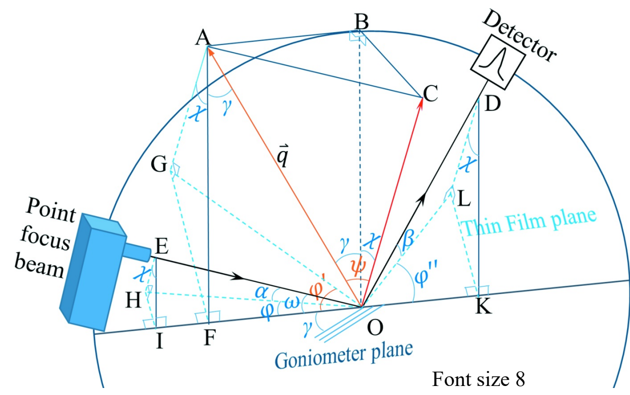

Figure 3

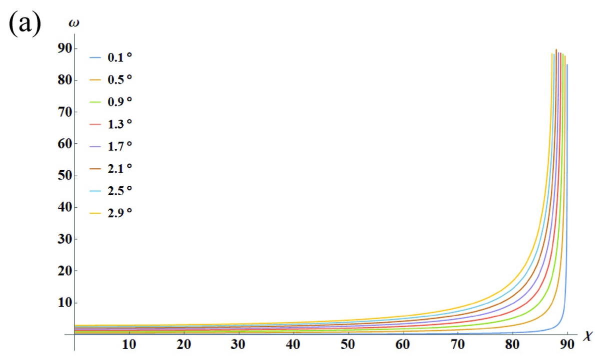

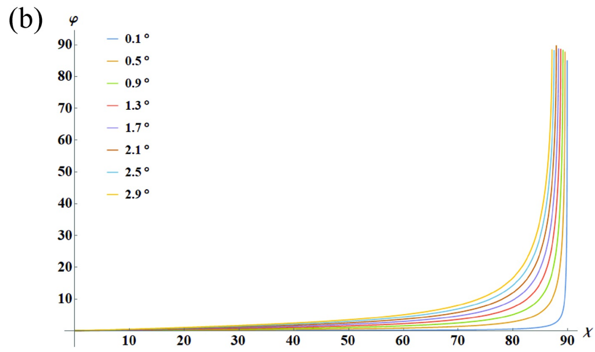

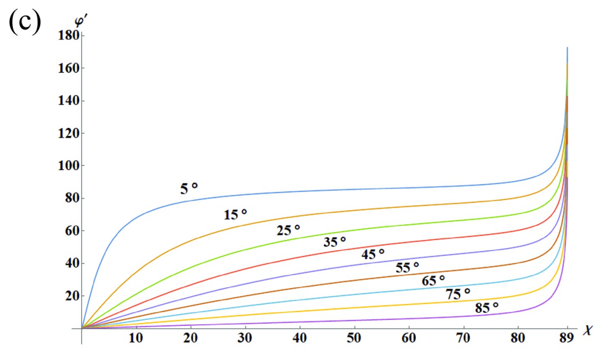

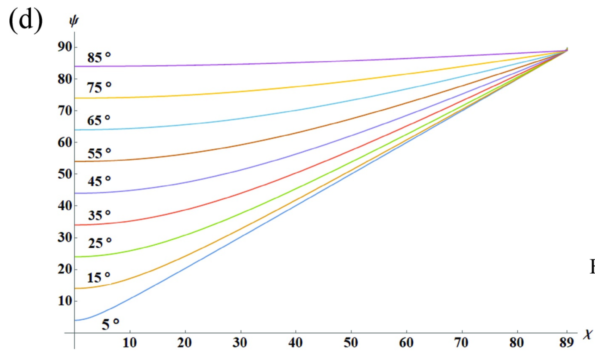

Font size 8

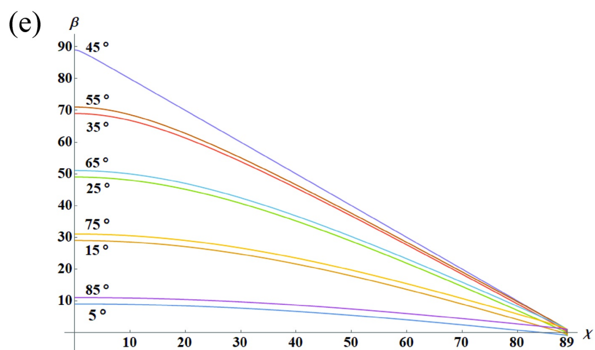

Figure 4

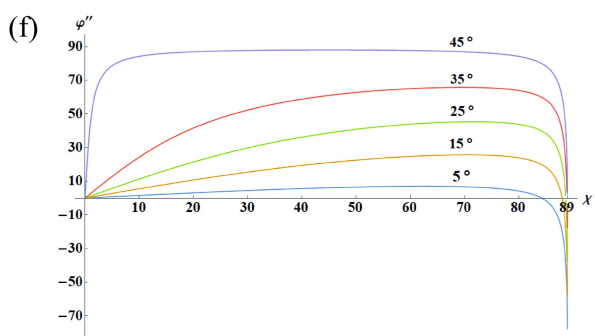

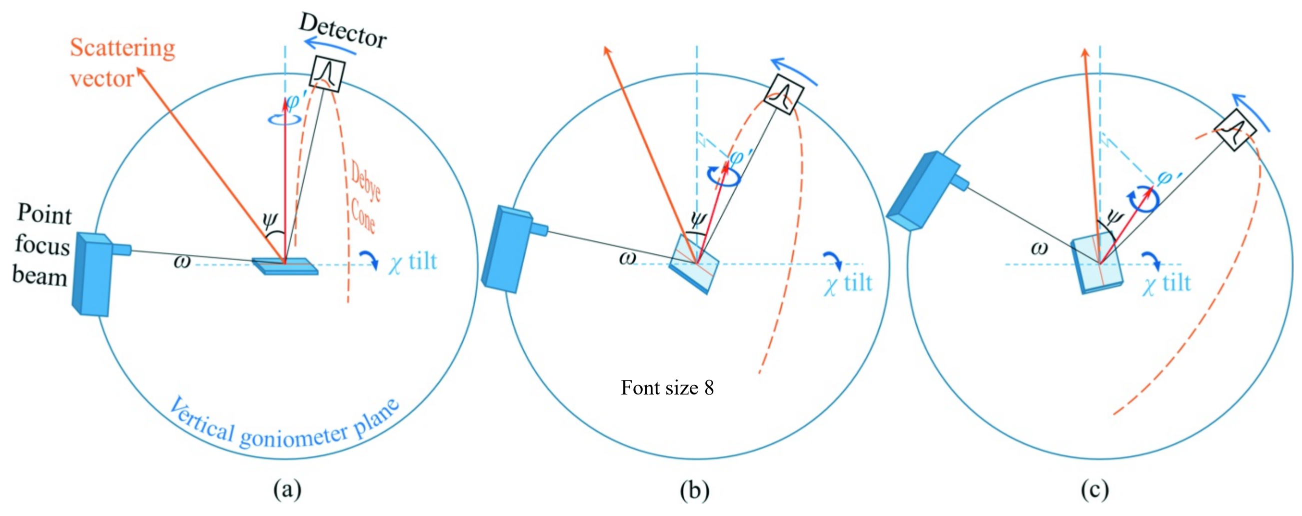

Figure 5

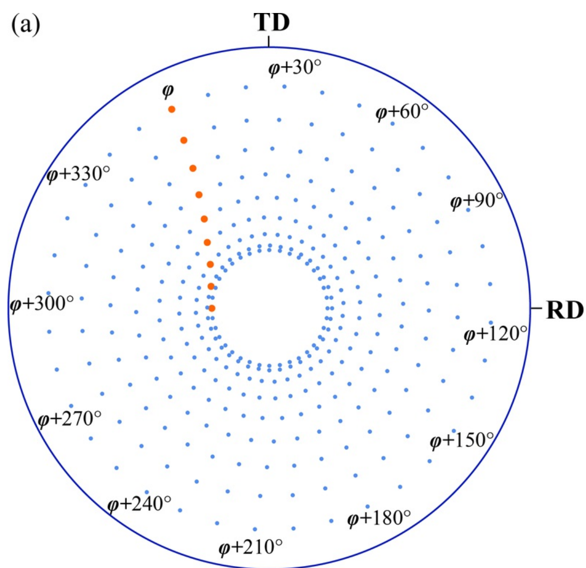

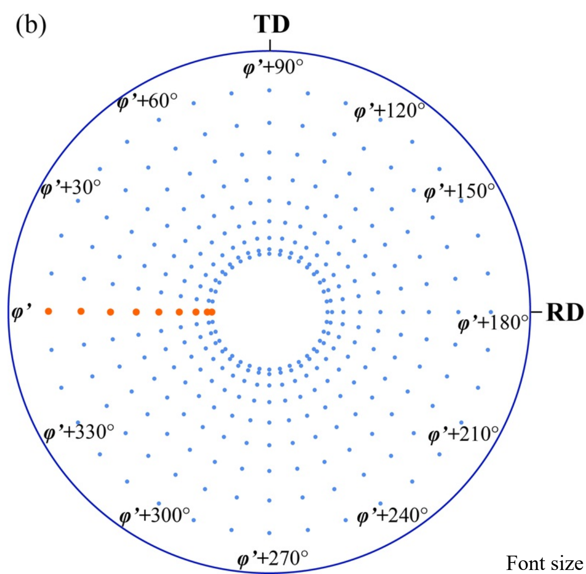

Font size 8

Figure 6

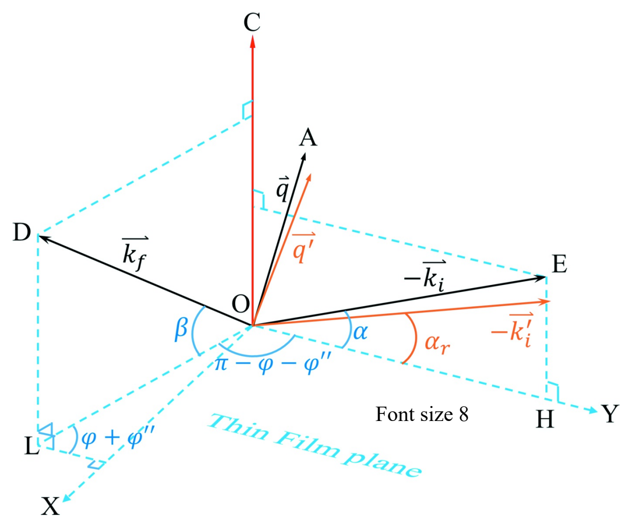

Figure 7

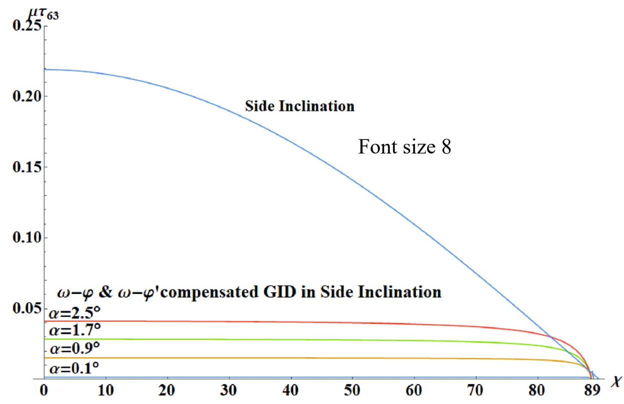

Figure 8

```
for idx_chi = 0 to 8
    set chi = idx_chi*10
    set Omega = Math.Asin(Math.Sin(Math.PI * Incident_Angle / 180.0) / Math.Cos(Math.PI *chi / 180.0))/Math.PI*180.0
    set psi = Math.Acos(Math.Cos(Math.PI * (Bragg - Omega) / 180.0) * Math.Cos(Math.PI * chi / 180.0))/Math.PI*180.0
    set phi1 = Math.Acos(Math.Max(-1, Math.Min(1, Math.Sin(Math.PI *(Bragg - Omega) / 180.0)  / Math.Sin(Math.PI *psi / 180.0))))/Math.PI*180.0
    for idx_phi = 0 to 35
        chi_pos.Append(chi)
        Omega_pos.Append(Omega)
        phi_pos.Append(phi1 + idx_phi*10)
        Logging.WriteToOutput("Chi/Omega/Phi Triplet: (" + chi.AsString() + ", " + Omega.AsString() + ", "+ (phi1 + idx_phi*10).AsString() + ")")
    end for
end for
```

Font size 8

Figure 9

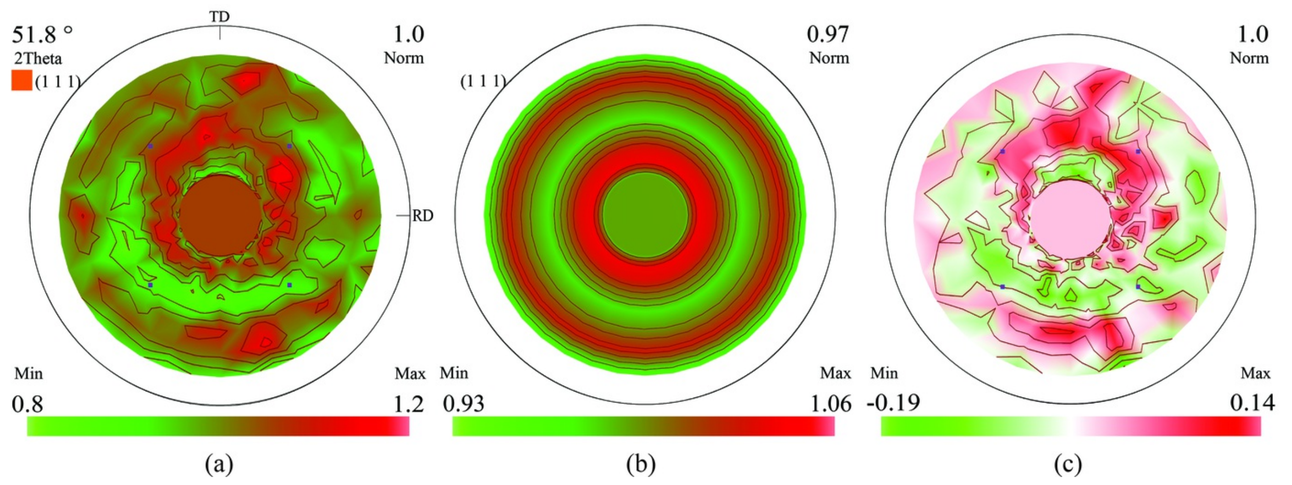

Figure 10

Font size 8

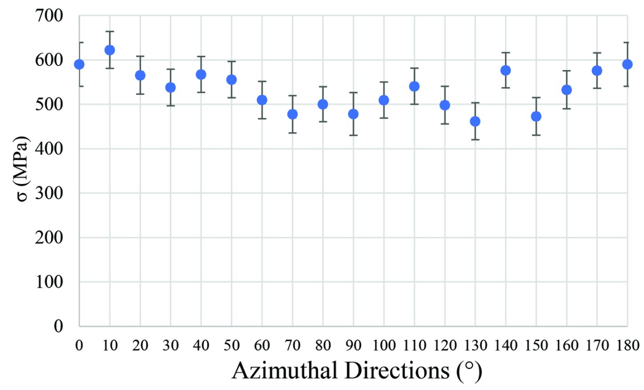

Figure 11

Font size 8

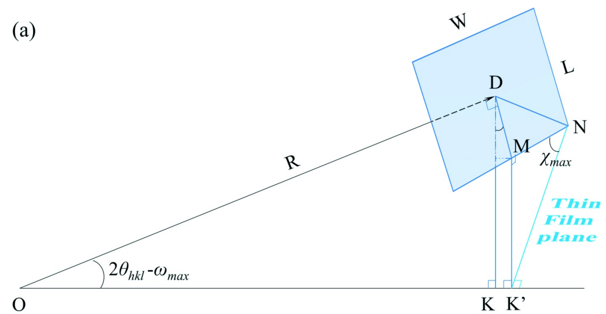

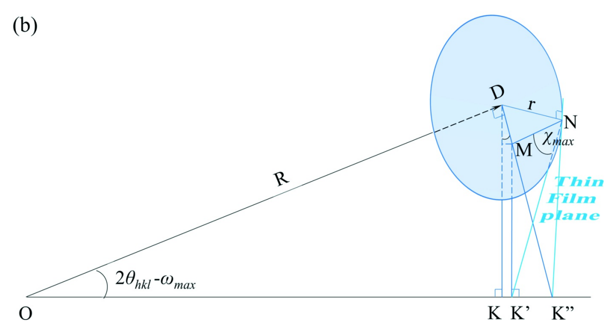

Figure 12

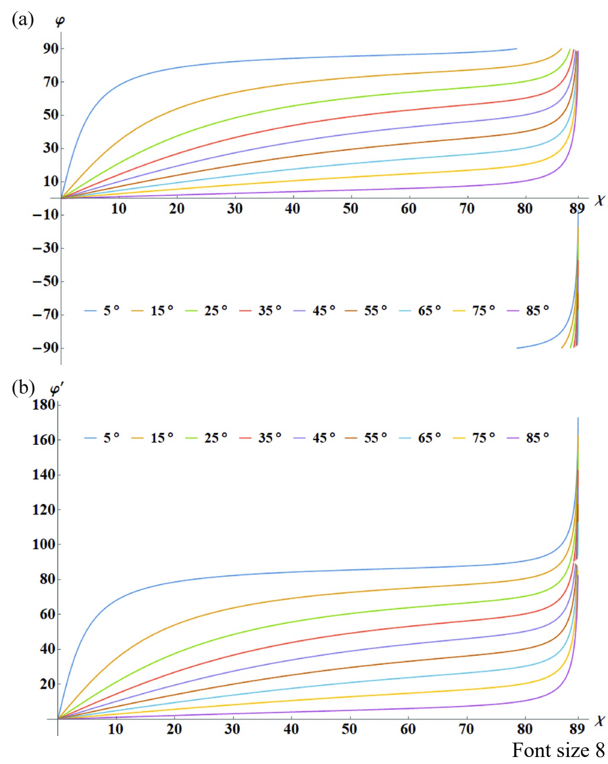

Figure 13

Figure 14

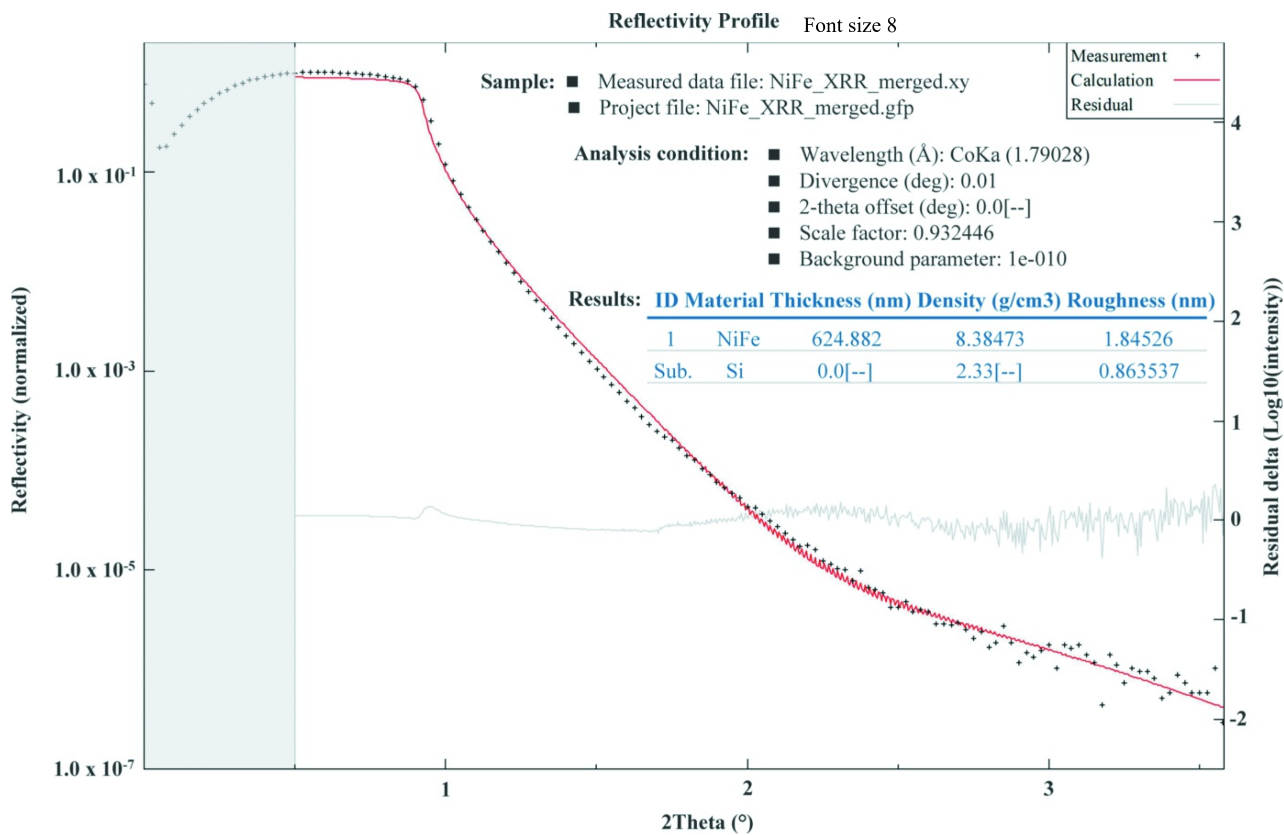

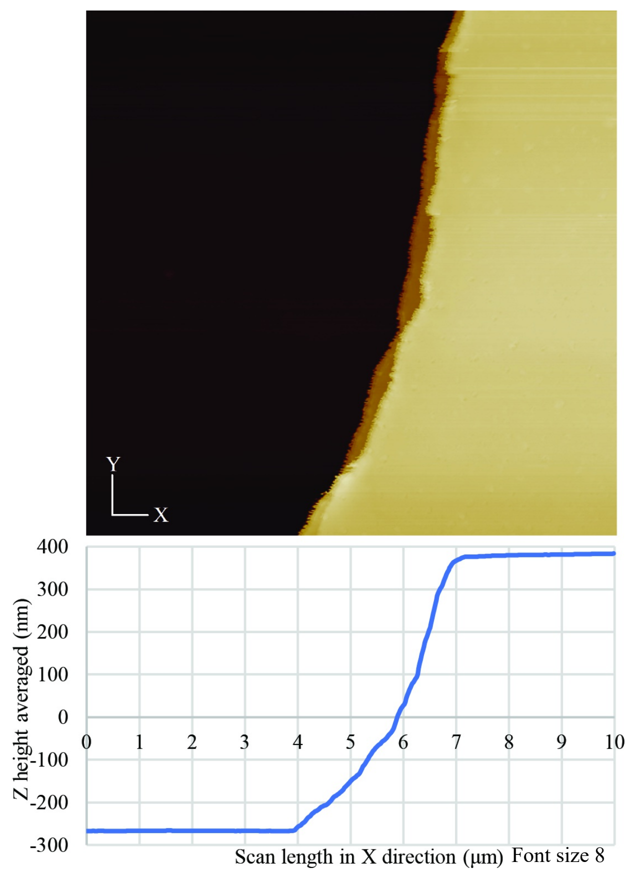

Figure 15

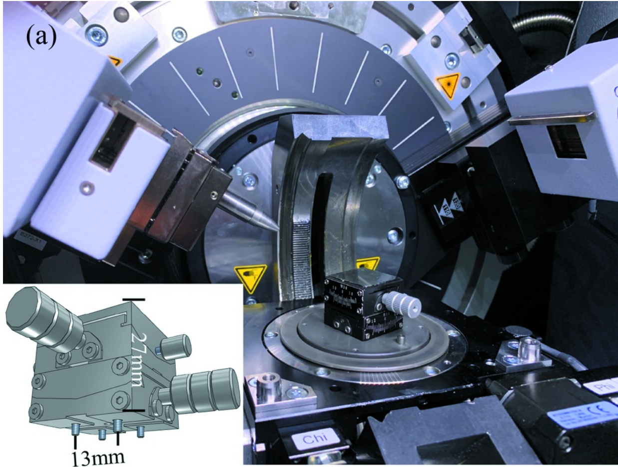

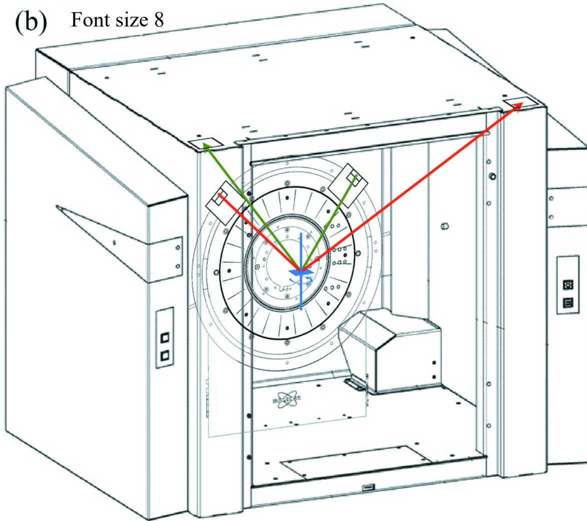

Figure 16